

Measurement of CP -Violating Asymmetries in the $B^0 \rightarrow K^+ K^- K_S^0$ Dalitz Plot

The *BABAR* Collaboration

August 5, 2008

Abstract

We present a preliminary measurement of CP -violation parameters in the decay $B^0 \rightarrow K^+ K^- K_S^0$, using approximately 465 million $B\bar{B}$ events collected by the *BABAR* detector at SLAC. Reconstructing the neutral kaon as $K_S^0 \rightarrow \pi^+ \pi^-$ or $K_S^0 \rightarrow \pi^0 \pi^0$, we analyze the Dalitz plot distribution and measure fractions to intermediate states. We extract CP parameters from the asymmetries in amplitudes and phases between B^0 and \bar{B}^0 decays across the Dalitz plot. From a fit to the whole Dalitz plot, we measure $\beta_{eff} = 0.44 \pm 0.07 \pm 0.02$, $A_{CP} = 0.03 \pm 0.07 \pm 0.02$, where the first uncertainties are statistical and the second ones are systematic. For decays to ϕK_S^0 , we measure $\beta_{eff} = 0.13 \pm 0.13 \pm 0.02$, $A_{CP} = 0.14 \pm 0.19 \pm 0.02$. For decays to $f_0 K_S^0$, we measure $\beta_{eff} = 0.15 \pm 0.13 \pm 0.03$, $A_{CP} = 0.01 \pm 0.26 \pm 0.07$. From a fit to the region of the Dalitz plot with $m_{K^+ K^-} > 1.1 \text{ GeV}/c^2$, we measure $\beta_{eff} = 0.52 \pm 0.08 \pm 0.03$, $A_{CP} = 0.05 \pm 0.09 \pm 0.04$.

Submitted to the 34th International Conference on High-Energy Physics, ICHEP 08,
29 July—5 August 2008, Philadelphia, Pennsylvania.

Stanford Linear Accelerator Center, Stanford University, Stanford, CA 94309

Work supported in part by Department of Energy contract DE-AC02-76SF00515.

The BABAR Collaboration,

B. Aubert, M. Bona, Y. Karyotakis, J. P. Lees, V. Poireau, E. Prencipe, X. Prudent, V. Tisserand
*Laboratoire de Physique des Particules, IN2P3/CNRS et Université de Savoie, F-74941 Annecy-Le-Vieux,
France*

J. Garra Tico, E. Grauges
Universitat de Barcelona, Facultat de Fisica, Departament ECM, E-08028 Barcelona, Spain

L. Lopez^{ab}, A. Palano^{ab}, M. Pappagallo^{ab}
INFN Sezione di Bari^a; Dipartimento di Fisica, Università di Bari^b, I-70126 Bari, Italy

G. Eigen, B. Stugu, L. Sun
University of Bergen, Institute of Physics, N-5007 Bergen, Norway

G. S. Abrams, M. Battaglia, D. N. Brown, R. N. Cahn, R. G. Jacobsen, L. T. Kerth, Yu. G. Kolomensky,
G. Lynch, I. L. Osipenkov, M. T. Ronan,¹ K. Tackmann, T. Tanabe
Lawrence Berkeley National Laboratory and University of California, Berkeley, California 94720, USA

C. M. Hawkes, N. Soni, A. T. Watson
University of Birmingham, Birmingham, B15 2TT, United Kingdom

H. Koch, T. Schroeder
Ruhr Universität Bochum, Institut für Experimentalphysik 1, D-44780 Bochum, Germany

D. Walker
University of Bristol, Bristol BS8 1TL, United Kingdom

D. J. Asgeirsson, B. G. Fulsom, C. Hearty, T. S. Mattison, J. A. McKenna
University of British Columbia, Vancouver, British Columbia, Canada V6T 1Z1

M. Barrett, A. Khan
Brunel University, Uxbridge, Middlesex UB8 3PH, United Kingdom

V. E. Blinov, A. D. Bukin, A. R. Buzykaev, V. P. Druzhinin, V. B. Golubev, A. P. Onuchin,
S. I. Serednyakov, Yu. I. Skovpen, E. P. Solodov, K. Yu. Todyshev
Budker Institute of Nuclear Physics, Novosibirsk 630090, Russia

M. Bondioli, S. Curry, I. Eschrich, D. Kirkby, A. J. Lankford, P. Lund, M. Mandelkern, E. C. Martin,
D. P. Stoker
University of California at Irvine, Irvine, California 92697, USA

S. Abachi, C. Buchanan
University of California at Los Angeles, Los Angeles, California 90024, USA

J. W. Gary, F. Liu, O. Long, B. C. Shen,¹ G. M. Vitug, Z. Yasin, L. Zhang
University of California at Riverside, Riverside, California 92521, USA

¹Deceased

V. Sharma

University of California at San Diego, La Jolla, California 92093, USA

C. Campagnari, T. M. Hong, D. Kovalskyi, M. A. Mazur, J. D. Richman

University of California at Santa Barbara, Santa Barbara, California 93106, USA

T. W. Beck, A. M. Eisner, C. J. Flacco, C. A. Heusch, J. Kroseberg, W. S. Lockman, A. J. Martinez,
T. Schalk, B. A. Schumm, A. Seiden, M. G. Wilson, L. O. Winstrom

University of California at Santa Cruz, Institute for Particle Physics, Santa Cruz, California 95064, USA

C. H. Cheng, D. A. Doll, B. Echenard, F. Fang, D. G. Hitlin, I. Narsky, T. Piatenko, F. C. Porter

California Institute of Technology, Pasadena, California 91125, USA

R. Andreassen, G. Mancinelli, B. T. Meadows, K. Mishra, M. D. Sokoloff

University of Cincinnati, Cincinnati, Ohio 45221, USA

P. C. Bloom, W. T. Ford, A. Gaz, J. F. Hirschauer, M. Nagel, U. Nauenberg, J. G. Smith, K. A. Ulmer,
S. R. Wagner

University of Colorado, Boulder, Colorado 80309, USA

R. Ayad,² A. Soffer,³ W. H. Toki, R. J. Wilson

Colorado State University, Fort Collins, Colorado 80523, USA

D. D. Altenburg, E. Feltresi, A. Hauke, H. Jasper, M. Karbach, J. Merkel, A. Petzold, B. Spaan, K. Wacker

Technische Universität Dortmund, Fakultät Physik, D-44221 Dortmund, Germany

M. J. Kobel, W. F. Mader, R. Nogowski, K. R. Schubert, R. Schwierz, A. Volk

Technische Universität Dresden, Institut für Kern- und Teilchenphysik, D-01062 Dresden, Germany

D. Bernard, G. R. Bonneaud, E. Latour, M. Verderi

Laboratoire Leprince-Ringuet, CNRS/IN2P3, Ecole Polytechnique, F-91128 Palaiseau, France

P. J. Clark, S. Playfer, J. E. Watson

University of Edinburgh, Edinburgh EH9 3JZ, United Kingdom

M. Andreotti^{ab}, D. Bettoni^a, C. Bozzi^a, R. Calabrese^{ab}, A. Cecchi^{ab}, G. Cibinetto^{ab}, P. Franchini^{ab},
E. Luppi^{ab}, M. Negrini^{ab}, A. Petrella^{ab}, L. Piemontese^a, V. Santoro^{ab}

INFN Sezione di Ferrara^a; Dipartimento di Fisica, Università di Ferrara^b, I-44100 Ferrara, Italy

R. Baldini-Ferroli, A. Calcaterra, R. de Sangro, G. Finocchiaro, S. Pacetti, P. Patteri, I. M. Peruzzi,⁴
M. Piccolo, M. Rama, A. Zallo

INFN Laboratori Nazionali di Frascati, I-00044 Frascati, Italy

A. Buzzo^a, R. Contri^{ab}, M. Lo Vetere^{ab}, M. M. Macri^a, M. R. Monge^{ab}, S. Passaggio^a, C. Patrignani^{ab},
E. Robutti^a, A. Santroni^{ab}, S. Tosi^{ab}

INFN Sezione di Genova^a; Dipartimento di Fisica, Università di Genova^b, I-16146 Genova, Italy

²Now at Temple University, Philadelphia, Pennsylvania 19122, USA

³Now at Tel Aviv University, Tel Aviv, 69978, Israel

⁴Also with Università di Perugia, Dipartimento di Fisica, Perugia, Italy

K. S. Chaisanguanthum, M. Morii

Harvard University, Cambridge, Massachusetts 02138, USA

A. Adametz, J. Marks, S. Schenk, U. Uwer

Universität Heidelberg, Physikalisches Institut, Philosophenweg 12, D-69120 Heidelberg, Germany

V. Klose, H. M. Lacker

Humboldt-Universität zu Berlin, Institut für Physik, Newtonstr. 15, D-12489 Berlin, Germany

D. J. Bard, P. D. Dauncey, J. A. Nash, M. Tibbetts

Imperial College London, London, SW7 2AZ, United Kingdom

P. K. Behera, X. Chai, M. J. Charles, U. Mallik

University of Iowa, Iowa City, Iowa 52242, USA

J. Cochran, H. B. Crawley, L. Dong, W. T. Meyer, S. Prell, E. I. Rosenberg, A. E. Rubin

Iowa State University, Ames, Iowa 50011-3160, USA

Y. Y. Gao, A. V. Gritsan, Z. J. Guo, C. K. Lae

Johns Hopkins University, Baltimore, Maryland 21218, USA

N. Arnaud, J. Béquilleux, A. D’Orazio, M. Davier, J. Firmino da Costa, G. Grosdidier, A. Höcker,
V. Lepeltier, F. Le Diberder, A. M. Lutz, S. Pruvot, P. Roudeau, M. H. Schune, J. Serrano, V. Sordini,⁵
A. Stocchi, G. Wormser

*Laboratoire de l’Accélérateur Linéaire, IN2P3/CNRS et Université Paris-Sud 11, Centre Scientifique
d’Orsay, B. P. 34, F-91898 Orsay Cedex, France*

D. J. Lange, D. M. Wright

Lawrence Livermore National Laboratory, Livermore, California 94550, USA

I. Bingham, J. P. Burke, C. A. Chavez, J. R. Fry, E. Gabathuler, R. Gamet, D. E. Hutchcroft, D. J. Payne,
C. Touramanis

University of Liverpool, Liverpool L69 7ZE, United Kingdom

A. J. Bevan, C. K. Clarke, K. A. George, F. Di Lodovico, R. Sacco, M. Sigamani

Queen Mary, University of London, London, E1 4NS, United Kingdom

G. Cowan, H. U. Flaecher, D. A. Hopkins, S. Paramesvaran, F. Salvatore, A. C. Wren

*University of London, Royal Holloway and Bedford New College, Egham, Surrey TW20 0EX, United
Kingdom*

D. N. Brown, C. L. Davis

University of Louisville, Louisville, Kentucky 40292, USA

A. G. Denig M. Fritsch, W. Gradl, G. Schott

Johannes Gutenberg-Universität Mainz, Institut für Kernphysik, D-55099 Mainz, Germany

⁵Also with Università di Roma La Sapienza, I-00185 Roma, Italy

K. E. Alwyn, D. Bailey, R. J. Barlow, Y. M. Chia, C. L. Edgar, G. Jackson, G. D. Lafferty, T. J. West,
J. I. Yi

University of Manchester, Manchester M13 9PL, United Kingdom

J. Anderson, C. Chen, A. Jawahery, D. A. Roberts, G. Simi, J. M. Tuggle

University of Maryland, College Park, Maryland 20742, USA

C. Dallapiccola, X. Li, E. Salvati, S. Saremi

University of Massachusetts, Amherst, Massachusetts 01003, USA

R. Cowan, D. Dujmic, P. H. Fisher, G. Sciolla, M. Spitznagel, F. Taylor, R. K. Yamamoto, M. Zhao
*Massachusetts Institute of Technology, Laboratory for Nuclear Science, Cambridge, Massachusetts 02139,
USA*

P. M. Patel, S. H. Robertson

McGill University, Montréal, Québec, Canada H3A 2T8

A. Lazzaro^{ab}, V. Lombardo^a, F. Palombo^{ab}

INFN Sezione di Milano^a; Dipartimento di Fisica, Università di Milano^b, I-20133 Milano, Italy

J. M. Bauer, L. Cremaldi R. Godang,⁶ R. Kroeger, D. A. Sanders, D. J. Summers, H. W. Zhao

University of Mississippi, University, Mississippi 38677, USA

M. Simard, P. Taras, F. B. Viaud

Université de Montréal, Physique des Particules, Montréal, Québec, Canada H3C 3J7

H. Nicholson

Mount Holyoke College, South Hadley, Massachusetts 01075, USA

G. De Nardo^{ab}, L. Lista^a, D. Monorchio^{ab}, G. Onorato^{ab}, C. Sciacca^{ab}

*INFN Sezione di Napoli^a; Dipartimento di Scienze Fisiche, Università di Napoli Federico II^b, I-80126
Napoli, Italy*

G. Raven, H. L. Snoek

*NIKHEF, National Institute for Nuclear Physics and High Energy Physics, NL-1009 DB Amsterdam, The
Netherlands*

C. P. Jessop, K. J. Knoepfel, J. M. LoSecco, W. F. Wang

University of Notre Dame, Notre Dame, Indiana 46556, USA

G. Benelli, L. A. Corwin, K. Honscheid, H. Kagan, R. Kass, J. P. Morris, A. M. Rahimi,

J. J. Regensburger, S. J. Sekula, Q. K. Wong

Ohio State University, Columbus, Ohio 43210, USA

N. L. Blount, J. Brau, R. Frey, O. Igonkina, J. A. Kolb, M. Lu, R. Rahmat, N. B. Sinev, D. Strom,

J. Strube, E. Torrence

University of Oregon, Eugene, Oregon 97403, USA

⁶Now at University of South Alabama, Mobile, Alabama 36688, USA

G. Castelli^{ab}, N. Gagliardi^{ab}, M. Margoni^{ab}, M. Morandin^a, M. Posocco^a, M. Rotondo^a, F. Simonetto^{ab},
R. Stroili^{ab}, C. Voci^{ab}

INFN Sezione di Padova^a; Dipartimento di Fisica, Università di Padova^b, I-35131 Padova, Italy

P. del Amo Sanchez, E. Ben-Haim, H. Briand, G. Calderini, J. Chauveau, P. David, L. Del Buono,
O. Hamon, Ph. Leruste, J. Ocariz, A. Perez, J. Prendki, S. Sitt

*Laboratoire de Physique Nucléaire et de Hautes Energies, IN2P3/CNRS, Université Pierre et Marie
Curie-Paris6, Université Denis Diderot-Paris7, F-75252 Paris, France*

L. Gladney

University of Pennsylvania, Philadelphia, Pennsylvania 19104, USA

M. Biasini^{ab}, R. Covarelli^{ab}, E. Manoni^{ab},

INFN Sezione di Perugia^a; Dipartimento di Fisica, Università di Perugia^b, I-06100 Perugia, Italy

C. Angelini^{ab}, G. Batignani^{ab}, S. Bettarini^{ab}, M. Carpinelli^{ab,7}, A. Cervelli^{ab}, F. Forti^{ab}, M. A. Giorgi^{ab},
A. Lusiani^{ac}, G. Marchiori^{ab}, M. Morganti^{ab}, N. Neri^{ab}, E. Paoloni^{ab}, G. Rizzo^{ab}, J. J. Walsh^a

*INFN Sezione di Pisa^a; Dipartimento di Fisica, Università di Pisa^b; Scuola Normale Superiore di Pisa^c,
I-56127 Pisa, Italy*

D. Lopes Pegna, C. Lu, J. Olsen, A. J. S. Smith, A. V. Telnov

Princeton University, Princeton, New Jersey 08544, USA

F. Anulli^a, E. Baracchini^{ab}, G. Cavoto^a, D. del Re^{ab}, E. Di Marco^{ab}, R. Faccini^{ab}, F. Ferrarotto^a,
F. Ferroni^{ab}, M. Gaspero^{ab}, P. D. Jackson^a, L. Li Gioi^a, M. A. Mazzoni^a, S. Morganti^a, G. Piredda^a,
F. Polci^{ab}, F. Renga^{ab}, C. Voena^a

INFN Sezione di Roma^a; Dipartimento di Fisica, Università di Roma La Sapienza^b, I-00185 Roma, Italy

M. Ebert, T. Hartmann, H. Schröder, R. Waldi

Universität Rostock, D-18051 Rostock, Germany

T. Adye, B. Franek, E. O. Olaiya, F. F. Wilson

Rutherford Appleton Laboratory, Chilton, Didcot, Oxon, OX11 0QX, United Kingdom

S. Emery, M. Escalier, L. Esteve, S. F. Ganzhur, G. Hamel de Monchenault, W. Kozanecki, G. Vasseur,
Ch. Yèche, M. Zito

CEA, Irfu, SPP, Centre de Saclay, F-91191 Gif-sur-Yvette, France

X. R. Chen, H. Liu, W. Park, M. V. Purohit, R. M. White, J. R. Wilson

University of South Carolina, Columbia, South Carolina 29208, USA

M. T. Allen, D. Aston, R. Bartoldus, P. Bechtel, J. F. Benitez, R. Cenci, J. P. Coleman, M. R. Convery,
J. C. Dingfelder, J. Dorfan, G. P. Dubois-Felsmann, W. Dunwoodie, R. C. Field, A. M. Gabareen,
S. J. Gowdy, M. T. Graham, P. Grenier, C. Hast, W. R. Innes, J. Kaminski, M. H. Kelsey, H. Kim, P. Kim,
M. L. Kocian, D. W. G. S. Leith, S. Li, B. Lindquist, S. Luitz, V. Luth, H. L. Lynch, D. B. MacFarlane,
H. Marsiske, R. Messner, D. R. Muller, H. Neal, S. Nelson, C. P. O'Grady, I. Ofte, A. Perazzo, M. Perl,
B. N. Ratcliff, A. Roodman, A. A. Salnikov, R. H. Schindler, J. Schwiening, A. Snyder, D. Su,
M. K. Sullivan, K. Suzuki, S. K. Swain, J. M. Thompson, J. Va'vra, A. P. Wagner, M. Weaver, C. A. West,
W. J. Wisniewski, M. Wittgen, D. H. Wright, H. W. Wulsin, A. K. Yarritu, K. Yi, C. C. Young, V. Ziegler

Stanford Linear Accelerator Center, Stanford, California 94309, USA

⁷Also with Università di Sassari, Sassari, Italy

P. R. Burchat, A. J. Edwards, S. A. Majewski, T. S. Miyashita, B. A. Petersen, L. Wilden
Stanford University, Stanford, California 94305-4060, USA

S. Ahmed, M. S. Alam, J. A. Ernst, B. Pan, M. A. Saeed, S. B. Zain
State University of New York, Albany, New York 12222, USA

S. M. Spanier, B. J. Wogslund
University of Tennessee, Knoxville, Tennessee 37996, USA

R. Eckmann, J. L. Ritchie, A. M. Ruland, C. J. Schilling, R. F. Schwitters
University of Texas at Austin, Austin, Texas 78712, USA

B. W. Drummond, J. M. Izen, X. C. Lou
University of Texas at Dallas, Richardson, Texas 75083, USA

F. Bianchi^{ab}, D. Gamba^{ab}, M. Pelliccioni^{ab}
INFN Sezione di Torino^a; Dipartimento di Fisica Sperimentale, Università di Torino^b, I-10125 Torino, Italy

M. Bomben^{ab}, L. Bosisio^{ab}, C. Cartaro^{ab}, G. Della Ricca^{ab}, L. Lanceri^{ab}, L. Vitale^{ab}
INFN Sezione di Trieste^a; Dipartimento di Fisica, Università di Trieste^b, I-34127 Trieste, Italy

V. Azzolini, N. Lopez-March, F. Martinez-Vidal, D. A. Milanes, A. Oyanguren
IFIC, Universitat de Valencia-CSIC, E-46071 Valencia, Spain

J. Albert, Sw. Banerjee, B. Bhuyan, H. H. F. Choi, K. Hamano, R. Kowalewski, M. J. Lewczuk,
I. M. Nugent, J. M. Roney, R. J. Sobie
University of Victoria, Victoria, British Columbia, Canada V8W 3P6

T. J. Gershon, P. F. Harrison, J. Ilic, T. E. Latham, G. B. Mohanty
Department of Physics, University of Warwick, Coventry CV4 7AL, United Kingdom

H. R. Band, X. Chen, S. Dasu, K. T. Flood, Y. Pan, M. Pierini, R. Prepost, C. O. Vuosalo, S. L. Wu
University of Wisconsin, Madison, Wisconsin 53706, USA

1 INTRODUCTION

We present a time-dependent analysis of the Dalitz plot (DP) in flavor tagged $B^0 \rightarrow K^+K^-K_S^0$ decays, with the K_S^0 reconstructed as $K_S^0 \rightarrow \pi^+\pi^-$ or $K_S^0 \rightarrow \pi^0\pi^0$ (unless otherwise stated, charge conjugates are implied throughout this paper). In the Standard Model (SM), these decays are dominated by $\rightarrow s\bar{s}s$ gluonic penguin amplitudes, with a single weak phase. Contributions from $b \rightarrow u\bar{q}q$ tree amplitudes, proportional to the Cabibbo-Kobayashi-Maskawa (CKM) matrix element V_{ub} with a CP -violating weak phase γ [1], are small, but may depend on the position in the Dalitz plot. In $B^0 \rightarrow \phi(K^+K^-)K^0$ decays the modification of the CP asymmetry due to the presence of suppressed tree amplitudes is at $\mathcal{O}(0.01)$ [2, 3], while at higher K^+K^- masses a larger contribution at $\mathcal{O}(0.1)$ is possible [4]. Therefore, to very good precision, we also expect the direct CP asymmetry for these decays to be small in the SM. The CP asymmetry in $B^0 \rightarrow K^+K^-K_S^0$ decay arises from the interference of decays and $B^0 \leftrightarrow \bar{B}^0$ mixing, with a relative phase of 2β . The Unitarity Triangle angle β has been measured in $B^0 \rightarrow [c\bar{c}]K^0$ decays to be $\sin 2\beta = 0.685 \pm 0.032$ [5, 6]. Current direct measurements favor the solution of $\beta = 0.37$ over $\beta = 1.20$ at the 98.3% C.L. [7, 8, 9, 10, 11, 12]. Furthermore, the $\beta = 0.37$ solution is the only one consistent with all indirect constraints [13, 14].

The decay $B^0 \rightarrow K^+K^-K_S^0$ is one of the most promising processes with which to search for physics beyond the SM. Since the leading amplitudes enter only at the one-loop level, additional contributions from heavy non-SM particles may be of comparable size. If the amplitude from heavy particles has a CP -violating phase, the measured CP -violation parameters may differ from those expected in the SM.

Previous *BABAR* measurements of the CP asymmetry in $B^0 \rightarrow K^+K^-K^0$ decays have been performed on $383 \times 10^6 B\bar{B}$ events [15]. This analysis updates that previous result with a larger dataset.

2 DATASET AND DETECTOR

The data used in this analysis were collected with the *BABAR* detector at the PEP-II asymmetric-energy B factory at SLAC. A total of 465 million $B\bar{B}$ pairs were used.

The *BABAR* detector is described in detail elsewhere [16]. Charged particle (track) momenta are measured with a 5-layer double-sided silicon vertex tracker (SVT) and a 40-layer drift chamber (DCH) coaxial with a 1.5-T superconducting solenoidal magnet. Neutral cluster (photon) positions and energies are measured with an electromagnetic calorimeter (EMC) consisting of 6580 CsI(Tl) crystals. Charged hadrons are identified with a detector of internally reflected Cherenkov light (DIRC) and specific ionization measurements (dE/dx) in the tracking detectors (DCH, SVT). Neutral hadrons that do not interact in the EMC are identified with detectors, up to 15 layers deep, in the flux return steel (IFR).

In addition to the data collected by *BABAR*, this analysis uses various samples of Monte Carlo (MC) events based on GEANT4 [17]. A sample of simulated $K^+K^-K_S^0$ events using a full Dalitz plot model based on *BABAR*'s previous measurement is used to study signal events, while backgrounds from B meson decays are studied using a separate sample of simulated events.

3 EVENT RECONSTRUCTION

We reconstruct $B^0 \rightarrow K^+K^-K_S^0$ decays by combining two oppositely charged tracks with a $K_S^0 \rightarrow \pi^+\pi^-$ or $K_S^0 \rightarrow \pi^0\pi^0$ candidate. The K^+ and K^- tracks must have at least 12 measured DCH

coordinates, a minimum transverse momentum of 0.1 GeV/c, and must originate from the nominal beam spot. Tracks are identified as kaons using a likelihood ratio that combines dE/dx measured in the SVT and DCH with the Cherenkov angle and number of photons measured in the DIRC. The K^\pm candidates are required to be loosely compatible with the kaon hypothesis if the K^+K^- invariant mass is less than 1.1 GeV/ c^2 , while a tighter compatibility is required in all other cases to further suppress background.

For all modes, the main source of background is random combinations of particles produced in events of the type $e^+e^- \rightarrow q\bar{q}$ ($q = u, d, s, c$) (continuum). Additional background from decays of B mesons to other final states ($B\bar{B}$ background), with and without charm particles, is estimated from MC events.

We use event-shape variables, computed in the center-of-mass (CM) frame, to separate continuum events with a jet-like topology from the more isotropic B decays. Continuum events are suppressed by requiring the quantity $|\cos\theta_T|$ to be less than 0.9, where θ_T is the angle between the thrust axis calculated with the B candidate's daughters and the thrust axis formed from the other charged and neutral particles in the event. Further discrimination comes from a Fisher discriminant (\mathcal{F}) based on 1) $\cos\theta_T$, 2) 0th and 2nd order Legendre moments $\mathcal{L}_{i=0,2} = \sum_j p_j |\cos(\theta_j)|^i$, where j is all tracks and clusters not used to reconstruct the B meson, p_j is their momentum, and θ_j is the angle to the B thrust axis, and 3) the magnitude of the cosine of the angle of the B with respect to the collision axis $|\cos\theta_B|$.

In a small fraction of events, more than one B candidate in a single event passes our selection criteria. In this case, a single best B candidate is selected based on the K_s^0 invariant mass and on the quality of the kaon tracks.

B candidates are identified using two kinematic variables that separate signal from continuum background. These are the beam-energy-substituted mass $m_{\text{ES}} \equiv \sqrt{(s/2 + \mathbf{p}_i \cdot \mathbf{p}_B)^2/E_i^2 - \mathbf{p}_B^2}$, where \sqrt{s} is the total e^+e^- CM energy, (E_i, \mathbf{p}_i) is the four-momentum of the initial e^+e^- system and \mathbf{p}_B is the B candidate momentum, both measured in the laboratory frame, and $\Delta E \equiv E_B - \sqrt{s}/2$, where E_B is the B candidate energy in the CM frame.

3.1 $B^0 \rightarrow K^+K^-K_s^0$, $K_s^0 \rightarrow \pi^+\pi^-$

For decays $B^0 \rightarrow K^+K^-K_s^0$ and $K_s^0 \rightarrow \pi^+\pi^-$, K_s^0 candidates are formed from oppositely charged tracks with an invariant mass within 20 MeV/ c^2 of the K_s^0 mass [1]. The K_s^0 vertex is required to be separated from the B^0 vertex by at least 3σ . The angle α_{K_s} between the K_s^0 momentum vector and the vector connecting the B^0 and K_s^0 vertices must satisfy $\cos\alpha_{K_s} > 0.999$. Distributions of the kinematic variables m_{ES} and ΔE in data, for signal and background events calculated using the *sPlot* event-weighting method [18], are shown in Fig. 1.

3.2 $B^0 \rightarrow K^+K^-K_s^0$, $K_s^0 \rightarrow \pi^0\pi^0$

For decays $B^0 \rightarrow K^+K^-K_s^0$ and $K_s^0 \rightarrow \pi^0\pi^0$, K_s^0 candidates are formed from two $\pi^0 \rightarrow \gamma\gamma$ candidates. Each of the four photons must have $E_\gamma > 0.05$ GeV and have a transverse shower shape loosely consistent with an electromagnetic shower. Additionally, we require each π^0 candidate to satisfy $0.100 < m_{\gamma\gamma} < 0.155$ GeV/ c^2 . The resulting $K_s^0 \rightarrow \pi^0\pi^0$ mass is required to satisfy $0.4776 < m_{\pi^0\pi^0} < 0.5276$ GeV/ c^2 . A K_s^0 mass constraint is then applied for the reconstruction of the B^0 candidate.

The kinematic variables m_{ES} and ΔE are formed for each candidate as in Sec. 3. Distributions of these variables in data, for signal and background events calculated using the *sPlot* event-weighting

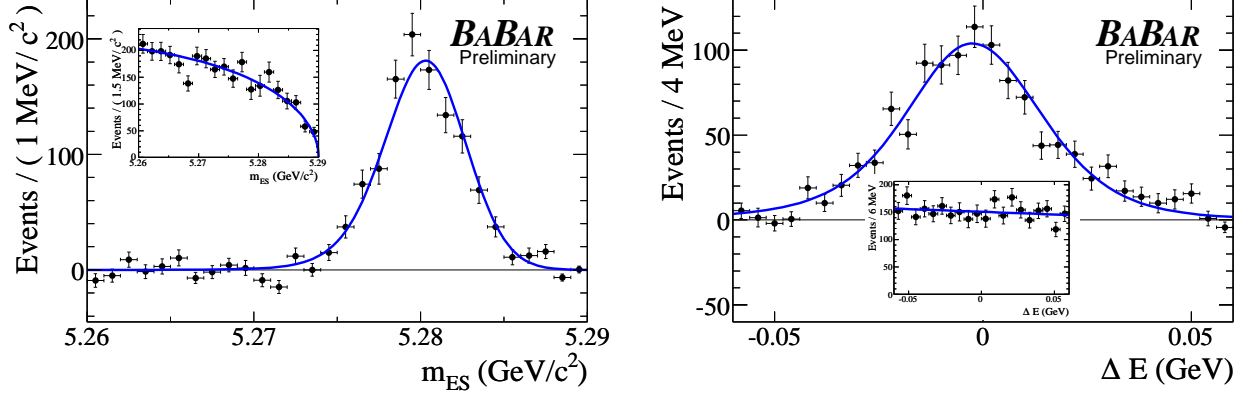


Figure 1: Distributions of kinematic variables (left) m_{ES} and (right) ΔE for the $K^+K^-K_S^0(\pi^+\pi^-)$ sample. The plots show signal, with the continuum background shown in the insets. The points are data events weighted with the $sPlot$ technique, while the curves are the PDF shapes used in the ML fit (Sec. 4).

method, are shown in Fig. 2. Note that the mean of the signal ΔE distribution is shifted from zero due to energy leakage in the EMC.

4 ANALYSIS OF THE DALITZ PLOT

Four-momentum conservation in a three-body decay gives the relation $M_{B^0}^2 + m_1^2 + m_2^2 + m_3^2 = m_{12}^2 + m_{13}^2 + m_{23}^2$, where $m_{ij}^2 = (p_i + p_j)^2$ is the square of the invariant mass of a daughter pair. This constraint leaves a choice of two independent Dalitz plot variables to describe the decay dynamics of a spin-zero particle. In this analysis we choose the K^+K^- invariant mass $m_{K^+K^-}$ and the cosine of the helicity angle between the K^+ and the K_S^0 in the K^+K^- center-of-mass frame, $\cos\theta_H$.

We perform an extended maximum likelihood fit to the measured time dependent Dalitz plot distribution. We first fit on the whole DP, then fit on the $m_{K^+K^-} > 1.1 \text{ GeV}/c^2$ range (High-mass), then fit on the $m_{K^+K^-} < 1.1 \text{ GeV}/c^2$ range (Low-mass). All fits are performed on the combined $K^+K^-K_S^0(\pi^+\pi^-)$ and $K^+K^-K_S^0(\pi^0\pi^0)$ samples simultaneously. The likelihood function \mathcal{L} for each subsample is defined as

$$\mathcal{L} = \exp\left(-\sum_i n_i\right) \prod_j \left[\sum_i n_i \mathcal{P}_{i,j}\right] \quad (1)$$

where i labels the different signal and background components, j runs over all events in the sample, and n_i is the event yield for events of the i -th component. The probability density function (PDF) \mathcal{P}_i of each component is defined as

$$\mathcal{P}_i \equiv \mathcal{P}_i(m_{ES}) \cdot \mathcal{P}_i(\Delta E) \cdot \mathcal{P}_i(\mathcal{F}) \cdot \mathcal{P}_{DP,i}(m_{K^+K^-}, \cos\theta_H, \Delta t, q_{tag}) \otimes \mathcal{R}_i(\Delta t, \sigma_{\Delta t}), \quad (2)$$

where q_{tag} is the flavor of the tagged B (1 for B^0 and -1 for \bar{B}^0), and $\Delta t = t_{rec} - t_{tag}$ is the difference of the proper decay times of the two B -mesons in the $\Upsilon(4S)$ decay. $\sigma_{\Delta t}$ is the error on Δt , and \mathcal{R} is the Δt resolution function determined from a high statistics independent sample [5]. For the purpose of calculating the DP coordinates $m_{K^+K^-}$ and $\cos\theta_H$, we refit the B candidates applying a B mass constraint. This ensures that the B candidates are reconstructed within the DP boundary.

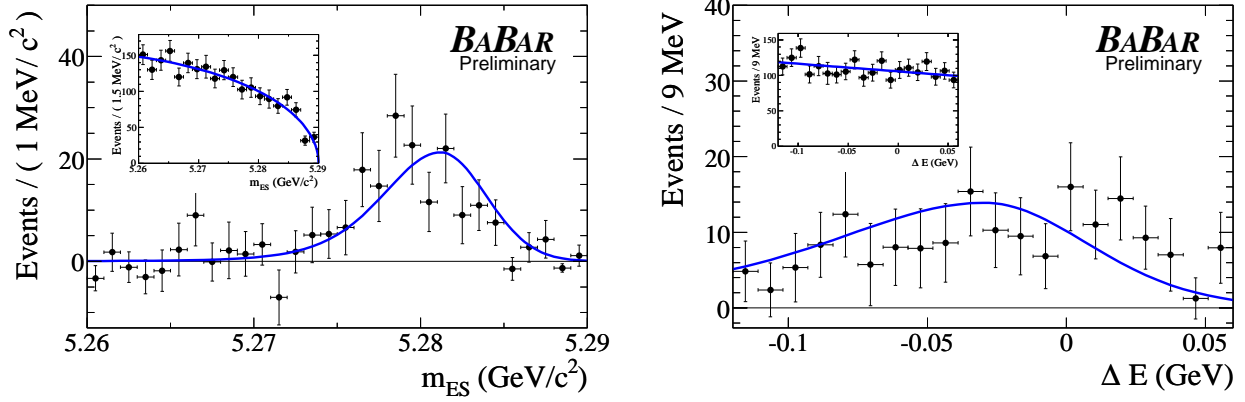


Figure 2: Distributions of kinematic variables (left) m_{ES} and (right) ΔE for the $K^+K^-K_S^0(\pi^0\pi^0)$ sample. The plots show signal, with the continuum background shown in the insets. The points are data events weighted with the $sPlot$ technique, while the curves are the PDF shapes used in the ML fit (Sec. 4).

The Fisher discriminant PDF, $\mathcal{P}(\mathcal{F})$, is only used in the Low-mass fit (see Sec. 5). Because the Fisher discriminant is highly correlated with the position on the DP, we do not use the Fisher discriminant PDF for the fit to the whole DP or for the High-mass fit. The Fisher distributions are shown in Fig. 3. The PDFs for the individual fit components are described in more detail below.

4.1 Background in the Time-Dependent Dalitz Plot

We have two background components in our fit: continuum and $B\bar{B}$ background. For the continuum background component, we use the ARGUS function [19] for $\mathcal{P}(m_{ES})$, and linear polynomial functions for $\mathcal{P}(\Delta E)$. The Δt distribution is described by a double-Gaussian resolution function convolved with a PDF of the following form:

$$\mathcal{P}(\Delta t) = f_{prompt}\delta(\Delta t) + (1 - f_{prompt})e^{-|\Delta t|/\tau_{bg}}, \quad (3)$$

which allows for background decays with both zero and non-zero lifetimes. The Dalitz plot for the continuum background is parameterized using a two-dimensional histogram PDF in the variables $m_{K^+K^-}$ and $\cos\theta_H$. The histogram is filled with candidates from the region $5.2 < m_{ES} < 5.26$ GeV/c^2 .

We estimate the amount of $B\bar{B}$ background from Monte Carlo events. The $B\bar{B}$ background is almost purely combinatorial and is a few percent of the total background. In the $K^+K^-K_S^0(\pi^+\pi^-)$ mode, the m_{ES} and ΔE PDFs for the $B\bar{B}$ backgrounds are parameterized with the same functional forms as the continuum backgrounds. Due to non-negligible correlation between m_{ES} and ΔE for $B\bar{B}$ background in the $K^+K^-K_S^0(\pi^0\pi^0)$ mode, we construct a two-dimensional smoothed histogram PDF in those variables. The Δt distribution is described with a PDF similar to the continuum backgrounds, but we also allow for the possibility that the non-zero lifetime component has a time-dependent CP asymmetry proportional to $\sin\Delta m_d\Delta t$ or $\cos\Delta m_d\Delta t$, where Δm_d is the mixing frequency of the B^0 meson. These asymmetries are set to zero in the nominal fit, but are varied as a systematic uncertainty. The Dalitz plot is described using a two-dimensional histogram PDF in a manner similar to the continuum backgrounds.

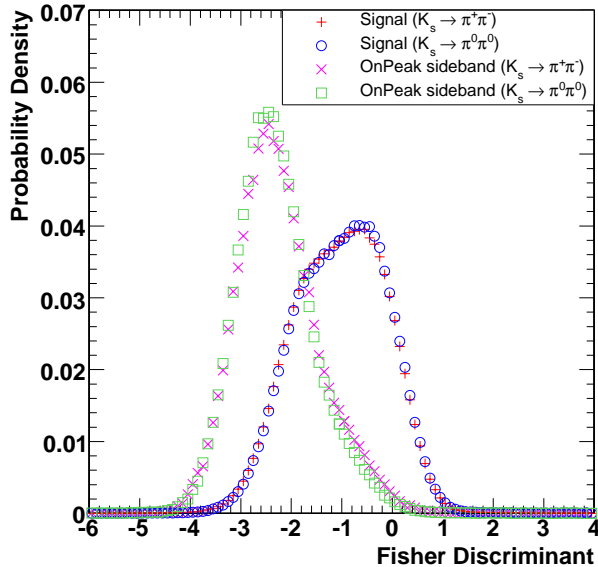


Figure 3: Fisher discriminant distributions for signal and continuum background and for $K^+K^-K_S^0(\pi^+\pi^-)$ sample and $K^+K^-K_S^0(\pi^0\pi^0)$ sample. Distributions are normalized to unit area.

4.2 Signal Decays in the Time-Dependent Dalitz Plot

The signal components of the PDFs for $\mathcal{P}(m_{ES})$ and $\mathcal{P}(\Delta E)$ are parameterized using modified Gaussian distributions: $\mathcal{P}(x) \propto \exp[-(x-x_0)^2/(2\sigma_{\pm}^2 + \alpha_{\pm}(x-x_0)^2)]$. We determine the parameters x_0 , σ_+ , σ_- , α_+ , and α_- using MC events, and fix them in fits to data. For $x < x_0$ ($x > x_0$), the parameters σ_- , α_- (σ_+ , α_+) are used.

For signal events, the time-dependence is a function of location in the DP. When the flavor of the tagged B q_{tag} , and the difference of the proper decay times Δt , are measured, the time- and flavor-dependent decay rate over the Dalitz plot can be written as

$$d\Gamma = \frac{1}{(2\pi)^3} \frac{1}{32M_{B^0}^3} \frac{e^{-|\Delta t|/\tau_{B^0}}}{4\tau_{B^0}} \times \left[|\mathcal{A}|^2 + |\bar{\mathcal{A}}|^2 + q_{tag} (1-2w) 2Im \left(e^{-2i\cdot\beta} \bar{\mathcal{A}}\mathcal{A}^* \right) \sin \Delta m_d \Delta t - q_{tag} (1-2w) \left(|\mathcal{A}|^2 - |\bar{\mathcal{A}}|^2 \right) \cos \Delta m_d \Delta t \right], \quad (4)$$

where $q_{tag} = +1(-1)$ when the other B meson is identified as a B^0 (\bar{B}^0) using a neural network technique [5]. The parameter w is the fraction of events in which the B meson is mistagged with the incorrect flavor, and the parameter β is the CKM angle β , coming from B^0 - \bar{B}^0 mixing. Approximately 75% of the signal events have tagging information and contribute to the measurement of CP violation parameters. After accounting for the mistag rate, the effective tagging efficiency is $(31.2 \pm 0.3)\%$. Events without tagging information are assigned a mistag rate of $w = 0.5$, and are included in the fit as they contribute to the determination of the Dalitz plot parameters. Decay amplitudes \mathcal{A} and $\bar{\mathcal{A}}$ are defined in (6) and (7) below. M_{B^0} , τ_{B^0} , and Δm_d are the mass, lifetime, and mixing frequency of the B^0 meson, respectively [1].

The PDF for the Dalitz plot rate takes the form

$$\mathcal{P}_{DP} \propto d\Gamma(m_{K^+K^-}, \cos \theta_H, \Delta t, q_{tag}) \cdot \varepsilon(m_{K^+K^-}, \cos \theta_H) \cdot |J| \otimes \mathcal{R}(\Delta t, \sigma_{\Delta t}), \quad (5)$$

where $|J(m_{K^+K^-})| = (2m_{K^+K^-})(2qp)$ is the Jacobian of the transformation $(m_{K^+K^-}^2, m_{K^+K_S^0}^2) \leftrightarrow (m_{K^+K^-}, \cos\theta_H)$, and is given in terms of the charged kaon momentum q and neutral kaon momentum p , in the K^+K^- frame. The efficiency ε is calculated from high-statistics samples of simulated events and depends on the position on the Dalitz plot.

The amplitude \mathcal{A} ($\bar{\mathcal{A}}$) for the decay $B^0 \rightarrow K^+K^-K_S^0$ ($\bar{B}^0 \rightarrow K^-K^+\bar{K}_S^0$) is, in our isobar model, written as a sum of decays through intermediate resonances:

$$\mathcal{A} = \sum_r c_r(1 + b_r)e^{i(\phi_r + \delta_r)} \cdot f_r, \quad \text{and} \quad (6)$$

$$\bar{\mathcal{A}} = \sum_r c_r(1 - b_r)e^{i(\phi_r - \delta_r)} \cdot \bar{f}_r. \quad (7)$$

The isobar coefficients c_r and ϕ_r are the magnitude and phase of the amplitude of component r , and we allow for different isobar coefficients for B^0 and \bar{B}^0 decays through the asymmetry parameters b_r and δ_r . The function $f_r = F_r \times T_r \times Z_r$ describes the dynamic properties of a resonance r , where F_r is the form-factor for the resonance decay vertex, T_r is the resonant mass-lineshape, and Z_r describes the angular distribution in the decay [20, 21].

Our model includes the $\phi(1020)$, for which we use the Blatt-Weisskopf centrifugal barrier factor $F_r = 1/\sqrt{1 + (Rq)^2}$ [20], where q is the daughter momentum in the resonance frame, and R is the effective meson radius, taken to be $R = 1.5 \text{ GeV}^{-1}$ (0.3 fm). For the scalar decays included in our model ($f_0(980)$, $X(1550)$, and χ_{c0}), we use a constant form-factor. Note that we have omitted a similar centrifugal factor for the B^0 decay vertex into the ϕK^0 intermediate state since its effect is negligible due to the small width of the $\phi(1020)$ resonance.

The angular distribution is constant for scalar decays, whereas for vector decays $Z \sim \vec{q} \cdot \vec{p}$, where \vec{q} is the momentum of the resonant daughter, and \vec{p} is the momentum of the third particle in the resonance frame. We describe the line-shape for the $\phi(1020)$, $X(1550)$, and χ_{c0} using the relativistic Breit-Wigner function

$$T(m) = \frac{1}{m_r^2 - m_{K^+K^-}^2 - im_r\Gamma(m)}, \quad (8)$$

where m_r is the resonance pole mass. The mass-dependent width is given as $\Gamma(m_{K^+K^-}) = \Gamma_r (q/q_r)^{2L+1} (m_r/m_{K^+K^-}) (F_r(q)/F_r(q_r))^2$, where L is the resonance spin and $q = q_r$ when $m_{K^+K^-} = m_r$. For the $\phi(1020)$ and χ_{c0} parameters, we use average measurements [1]. The $X(1550)$ is less well-established. Previous Dalitz plot analyses of $B^+ \rightarrow K^+K^+K^-$ [22, 24] and $B^0 \rightarrow K^+K^-K^0$ decays [25] report observations of a scalar resonance at around $1.5 \text{ GeV}/c^2$. The scalar nature has been confirmed by partial-wave analyses [23, 24]. However, previous measurements report inconsistent resonant widths: $0.145 \pm 0.029 \text{ GeV}/c^2$ [22] and $0.257 \pm 0.033 \text{ GeV}/c^2$ [24]. Branching fractions also disagree, so the nature of this component is still unclear [26]. In our nominal fit, we take the resonance parameters from Ref. [24], which is based on a larger sample of $B\bar{B}$ decays than Ref. [22], and consider the narrower width given in the latter in the systematic error studies.

The $f_0(980)$ resonance is described with the coupled-channel (Flatté) function

$$T(m_{K^+K^-}) = \frac{1}{m_r^2 - m_{K^+K^-}^2 - im_r(\rho_K g_K + \rho_\pi g_\pi)}, \quad (9)$$

where $\rho_K(m_{K^+K^-}) = 2\sqrt{1 - 4m_K^2/m_{K^+K^-}^2}$, $\rho_\pi(m_{K^+K^-}) = 2\sqrt{1 - 4m_\pi^2/m_{K^+K^-}^2}$, and the coupling strengths for the KK and $\pi\pi$ channels are taken as $g_\pi = 0.165 \pm 0.018 \text{ GeV}/c^2$, $g_K/g_\pi = 4.21 \pm 0.33$, and $m_r = 0.965 \pm 0.010 \text{ GeV}/c^2$ [27].

In addition to resonant decays, we include non-resonant amplitudes. Existing models consider contributions from contact terms or higher-resonance tails [28, 29, 4], but they do not capture features observed in data. We rely on a phenomenological parameterization [22] and describe the non-resonant terms as

$$\mathcal{A}_{NR}(\bar{\mathcal{A}}_{NR}) = \left(c_{12}e^{i\phi_{12}}e^{-\alpha m_{12}^2} + c_{13}e^{i\phi_{13}}e^{-\alpha m_{13}^2} + c_{23}e^{i\phi_{23}}e^{-\alpha m_{23}^2} \right) \cdot (1 \pm b_{NR}) \cdot e^{\pm i\delta_{NR}}, \quad (10)$$

where 1,2,3 denote the three daughter particles of the B meson. The slope of the exponential function is consistent among previous measurements in both neutral and charged B decays into three kaons [22, 24, 25], and we use $\alpha = 0.14 \pm 0.02 \text{ GeV}^{-2} \cdot c^4$.

We compute the direct CP -asymmetry parameters for resonance r from the asymmetries in amplitudes (b_r) and phases (δ_r) given in Eqs. (6, 7). We define the rate asymmetry as

$$A_{CP}(r) = \frac{|\bar{\mathcal{A}}_r|^2 - |\mathcal{A}_r|^2}{|\bar{\mathcal{A}}_r|^2 + |\mathcal{A}_r|^2} = \frac{-2b_r}{1 + b_r^2}, \quad (11)$$

and $\beta_{\text{eff}}(r) = \beta + \delta_r$ is defined as the total phase asymmetry. These asymmetries are related to the CP asymmetry parameters C and $-\eta S$ using the approximations

$$C_r \approx -A_{CP}(r), \quad \text{and} \quad (12)$$

$$-\eta_r S_r \approx \frac{1 - b_r^2}{1 + b_r^2} \sin(2\beta_{\text{eff}}(r)), \quad (13)$$

where η_r is the CP eigenvalue of the final state. The fraction for resonance r is computed as

$$\mathcal{F}_r = \frac{\int d \cos \theta_H dm_{K^+K^-} \cdot |J| \cdot (|\mathcal{A}_r|^2 + |\bar{\mathcal{A}}_r|^2)}{\int d \cos \theta_H dm_{K^+K^-} \cdot |J| \cdot (|\mathcal{A}|^2 + |\bar{\mathcal{A}}|^2)}. \quad (14)$$

The sum of the fractions can be different from unity due to interference between the isobars.

In addition to the previously mentioned resonances, the decays $B^0 \rightarrow D^+K^-$ ($D^+ \rightarrow K^+K_s^0$) and $B^0 \rightarrow D_s^+K^-$ ($D_s^+ \rightarrow K^+K_s^0$) are also counted as signal. We include non-interfering amplitudes for these modes in our Dalitz plot model, parameterizing the $D_{(s)}$ mesons on the Dalitz plot as Gaussian distributions with widths taken from studies of simulated events. The parameters b_r and δ_r are fixed to zero for the decays $B^0 \rightarrow D^+K^-$, $B^0 \rightarrow D_s^+K^-$, and $B^0 \rightarrow \chi_{c0}K_s^0$ throughout this analysis.

5 RESULTS

In order to determine parameters of the Dalitz plot model, we perform three fits: 1) whole DP fit, 2) Low-mass ($m_{K^+K^-} < 1.1 \text{ GeV}/c^2$) region fit, and 3) High-mass ($m_{K^+K^-} > 1.1 \text{ GeV}/c^2$) region fit.

5.1 The whole Dalitz Plot fit

We perform a fit to both 4316 $B^0 \rightarrow K^+K^-K_s^0(\pi^+\pi^-)$ and 2205 $B^0 \rightarrow K^+K^-K_s^0(\pi^0\pi^0)$ candidates simultaneously in the full Dalitz plot. In this step we assume that all charmless decays have the same CP -asymmetry parameters. A Fisher discriminant cut ($-2.5 < \mathcal{F} < 4$), which retains about 95% of signal events and 60% of continuum events, is applied. We do not include the Fisher PDF

in the fit. We vary the event yields, isobar coefficients, and the two CP -asymmetry parameters A_{CP} and β_{eff} averaged over the Dalitz plot. We find a signal yield of 1268 ± 43 ($K^+K^-K_S^0(\pi^+\pi^-)$) and 160 ± 19 ($K^+K^-K_S^0(\pi^0\pi^0)$) events, and a $B\bar{B}$ background yield of 47 ± 31 ($K^+K^-K_S^0(\pi^+\pi^-)$) and 24 ± 16 ($K^+K^-K_S^0(\pi^0\pi^0)$) events. The isobar amplitudes, phases, and fractions are listed in Table 1. The resonant fractions do not add up to 100% due to interference between the resonances. The CP -asymmetry parameters, and the correlation coefficients ρ between them, are summarized in Table 2. Fig. 4 shows a projection of the Dalitz plot variable m_{K+K^-} . Fig. 5 shows distributions of Δt for B^0 -tagged and \bar{B}^0 -tagged events, and the asymmetry $\mathcal{A}(\Delta t) = (N_{B^0} - N_{\bar{B}^0}) / (N_{B^0} + N_{\bar{B}^0})$, obtained with the $sPlot$ technique.

To calculate the significance of the nominal β_{eff} result, many fits are performed with fixed but different β_{eff} values. The change in likelihood as a function of β_{eff} is shown in Fig. 6.

Decay	Amplitude c_r	Phase ϕ_r	Fraction \mathcal{F}_r (%)
$\phi(1020)K_S^0$	0.00897 ± 0.00096	-0.341 ± 0.232	12.6 ± 1.0
$f_0(980)K_S^0$	0.542 ± 0.044	-0.201 ± 0.157	27.8 ± 7.1
$X_0(1550)K_S^0$	0.141 ± 0.017	-0.370 ± 0.154	5.70 ± 1.70
NR (K^+K^-)	1 (fixed)	0 (fixed)	98.1 ± 18.7
($K^+K_S^0$)	0.328 ± 0.058	1.81 ± 0.23	10.5 ± 3.4
($K^-K_S^0$)	0.353 ± 0.066	-1.44 ± 0.27	12.1 ± 3.8
$\chi_{c0}K_S^0$	0.0298 ± 0.0046	0.732 ± 0.437	2.53 ± 0.60
D^+K^-	1.34 ± 0.19	–	3.43 ± 0.69
$D_s^+K^-$	0.826 ± 0.160	–	1.37 ± 0.46

Table 1: Isobar amplitudes and phases from the fit to the whole DP. Three rows for non-resonant (NR) contribution correspond to coefficients of exponential functions in Eq. (10). The errors are statistical only.

Name	Whole DP	High-mass
A_{CP}	$0.03 \pm 0.07 \pm 0.02$	$0.05 \pm 0.09 \pm 0.04$
β_{eff}	$0.44 \pm 0.07 \pm 0.02$	$0.52 \pm 0.08 \pm 0.03$
ρ	0.041	0.031

Table 2: The CP -asymmetry parameters from the whole DP fit and the High-mass region fit. The first error is statistical and the second is systematic. ρ is the correlation coefficient.

5.2 High-mass fit

We perform a fit to both 3112 $B^0 \rightarrow K^+K^-K_S^0(\pi^+\pi^-)$ and 1917 $B^0 \rightarrow K^+K^-K_S^0(\pi^0\pi^0)$ candidates in the High-mass region ($m_{K+K^-} > 1.1 \text{ GeV}/c^2$) simultaneously. We fix all isobar coefficients to the values from the whole DP fit. We vary yields and shared CP -asymmetry parameters. We find a signal yield of 894 ± 36 $K^+K^-K_S^0(\pi^+\pi^-)$ and 117 ± 16 $K^+K^-K_S^0(\pi^0\pi^0)$ events, and a $B\bar{B}$ background yield of 50 ± 31 ($K^+K^-K_S^0(\pi^+\pi^-)$) and 20 ± 15 ($K^+K^-K_S^0(\pi^0\pi^0)$) events. The fit results are summarized in Table 2. Fig. 7 shows a projection of the Dalitz plot variable $\cos\theta_H$ for events in this region, using the $sPlot$ technique.

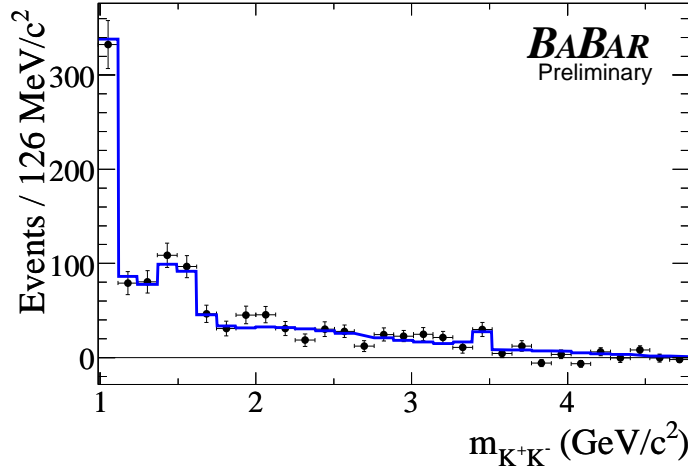


Figure 4: For the whole DP region fit, the distribution of the Dalitz plot variable $m_{K^+K^-}$ for signal-weighted data events (points) compared with the fit PDF in the $K^+K^-K_S^0(\pi^+\pi^-)$ mode.

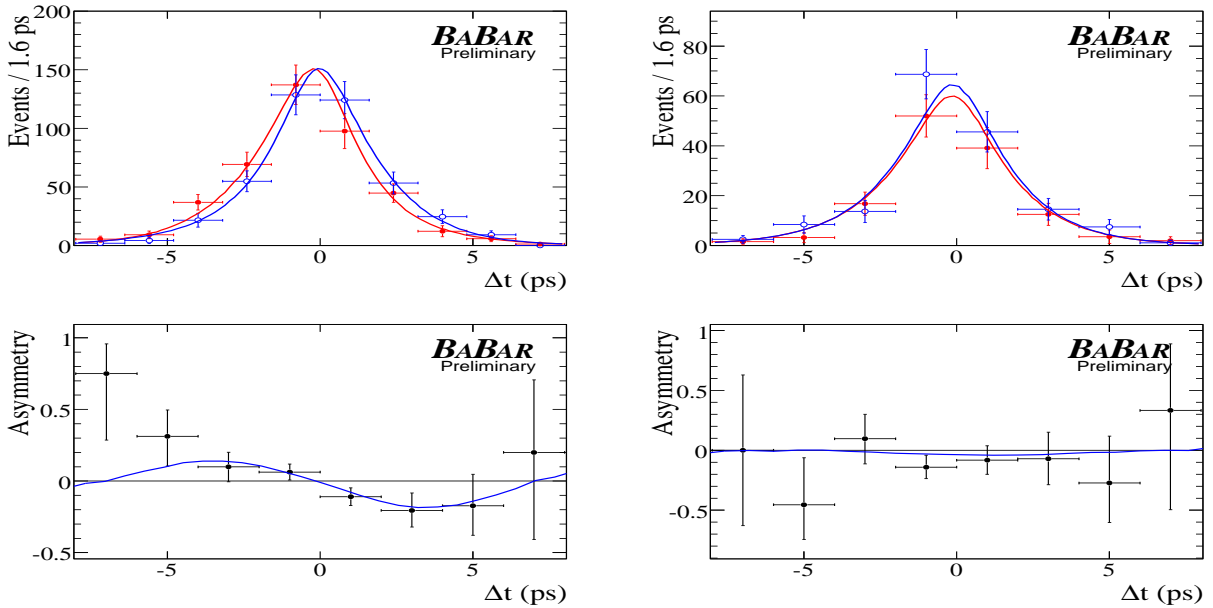
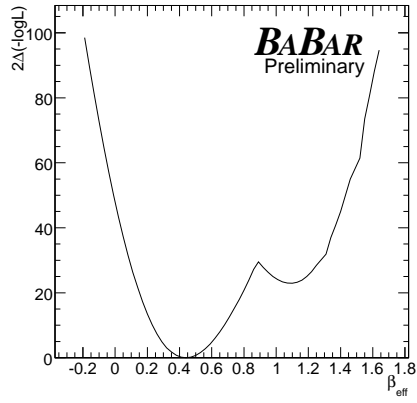
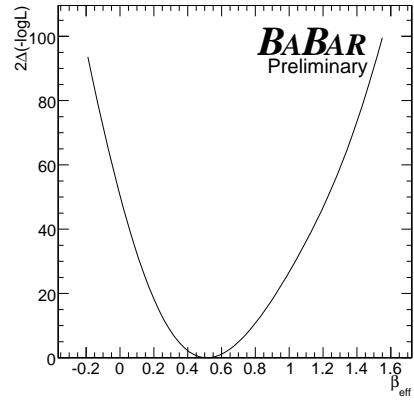


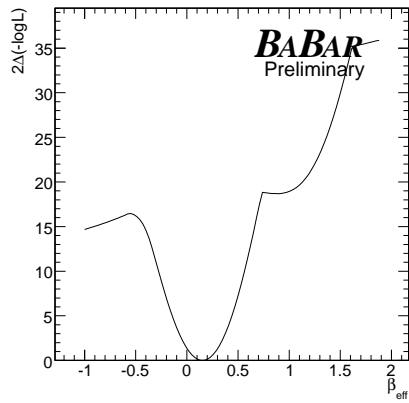
Figure 5: The Δt (top) distributions and asymmetries (bottom) in the whole DP (left) and Low-mass region (right), for the $K^+K^-K_S^0(\pi^+\pi^-)$ mode. For the Δt distributions, B^0 - (\bar{B}^0 -) tagged signal-weighted events are shown as filled (open) circles, with the PDF projection in dashed red (solid blue).



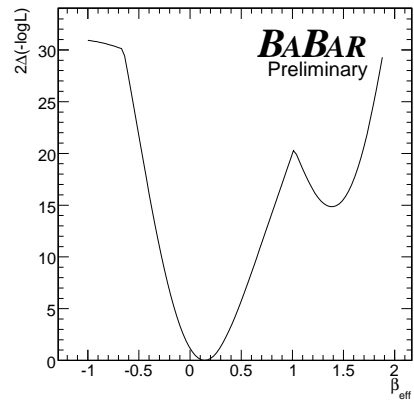
(a)



(b)



(c)



(d)

Figure 6: The change in the value of $-2\log(\mathcal{L})$ as a function of β_{eff} , for (a) the whole DP, (b) the High-mass region, (c) $f_0(980)$, and (d) $\phi(1020)$.

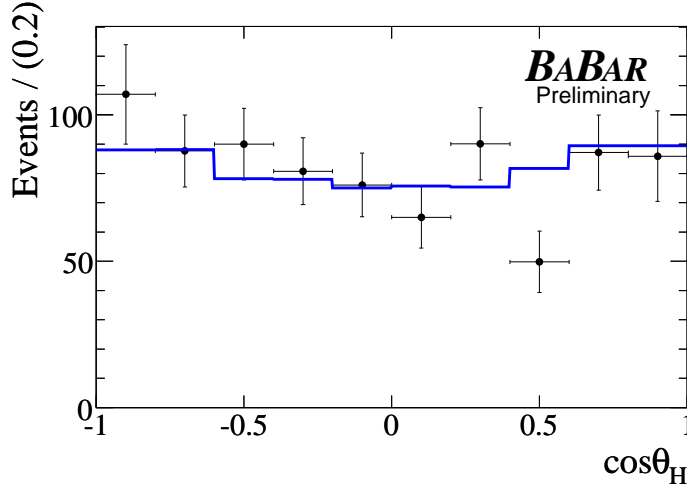


Figure 7: For the High-mass region fit, the distribution of the Dalitz plot variable $\cos\theta_H$ for signal-weighted data events (points) compared with the fit PDF in the $K^+K^-K_S^0(\pi^+\pi^-)$ mode.

5.3 Low-mass fit

In order to measure CP -asymmetry parameters for components with low- K^+K^- mass with reduced model-dependence from the rest of the DP, we select events using a cut of $m_{K^+K^-} < 1.1 \text{ GeV}/c^2$. Because we are only selecting a small region of the DP, the correlation between the Fisher discriminant \mathcal{F} and the DP location is unimportant. We therefore relax the cut on \mathcal{F} , and add the \mathcal{F} PDF to the fit. After these requirements on $m_{K^+K^-}$ and \mathcal{F} , there are 1846 ($K^+K^-K_S^0(\pi^+\pi^-)$) and 493 ($K^+K^-K_S^0(\pi^0\pi^0)$) candidates remaining. The most significant contributions in this region come from $\phi(1020)K_S^0$ and $f_0(980)K_S^0$ decays, with a smaller contribution from a low- K^+K^- mass tail of non-resonant decays. We fix all the isobar coefficients except for those of the $\phi(1020)$ to the values from the whole DP fit, and fix the CP -asymmetry parameters b_r and δ_r for all resonances except the $\phi(1020)$ and $f_0(980)$ to be 0. We vary the events yields, isobar coefficients for the $\phi(1020)$, and separate CP -asymmetry parameters for the $\phi(1020)$ and $f_0(980)$ in the fit. We find signal yields of 381 ± 23 ($K^+K^-K_S^0(\pi^+\pi^-)$) and 40 ± 9 ($K^+K^-K_S^0(\pi^0\pi^0)$) events, and $B\bar{B}$ background yields of 12 ± 13 ($K^+K^-K_S^0(\pi^+\pi^-)$) and -3 ± 5 ($K^+K^-K_S^0(\pi^0\pi^0)$) events.

The CP -asymmetry results are listed in Table 3; the systematic uncertainties will be described in Sec. 6. We find two solutions with likelihood difference $\Delta\log(\mathcal{L}) = 0.1$. Solution (1) is consistent with the SM, while Solution (2) has a value of β_{eff} for the $f_0(980)K_S^0$ decay that differs significantly from the SM, as shown in Table 3. The two solutions also have significantly different values of c_r for the $\phi(1020)$. Both solutions also have a mathematical ambiguity of $\pm\pi$ radians on β_{eff} for the $\phi(1020)$, and a correlated ambiguity of $\pm\pi$ radians on the isobar parameter ϕ_r for the $\phi(1020)$. This ambiguity is present because the decay amplitude contains interference terms that only depend on the linear combinations $\beta_{eff} + \phi_r$ and $\beta_{eff} - \phi_r$. We choose Solution (1) as our nominal solution. The correlation coefficients ρ between the CP parameters for Solution (1) are shown in Table 3. Because the decay rate depends on interference terms between the $\phi(1020)K_S^0$ and $f_0(980)K_S^0$ decays, the significant correlation between the measured CP parameters is expected.

Fig. 8 shows projections of the Dalitz plot distributions of events in this region, using the $sPlot$ technique. Fig. 5 shows distributions of Δt for B^0 -tagged and \bar{B}^0 -tagged events, and the asymmetry $\mathcal{A}(\Delta t) = (N_{B^0} - N_{\bar{B}^0}) / (N_{B^0} + N_{\bar{B}^0})$.

The decay $B^0 \rightarrow \phi(1020)K_S^0$, with highly suppressed tree amplitudes, is, in terms of theoretical

Name	Solution (1)	Solution (2)	Correlation			
			1	2	3	4
1 $A_{CP}(\phi K_S^0)$	$0.14 \pm 0.19 \pm 0.02$	0.13 ± 0.18	1.0	-0.09	-0.28	0.09
2 $\beta_{eff}(\phi K_S^0)$	$0.13 \pm 0.13 \pm 0.02$	0.14 ± 0.14		1.0	0.54	0.65
3 $A_{CP}(f_0 K_S^0)$	$0.01 \pm 0.26 \pm 0.07$	-0.49 ± 0.25			1.0	0.25
4 $\beta_{eff}(f_0 K_S^0)$	$0.15 \pm 0.13 \pm 0.03$	3.44 ± 0.19				1.0

Table 3: CP -violation parameters for $B^0 \rightarrow K^+ K^- K_S^0$ for $m_{K^+ K^-} < 1.1 \text{ GeV}/c^2$. The first error is statistical and the second is systematic. Correlation coefficients are given for Solution (1) only.

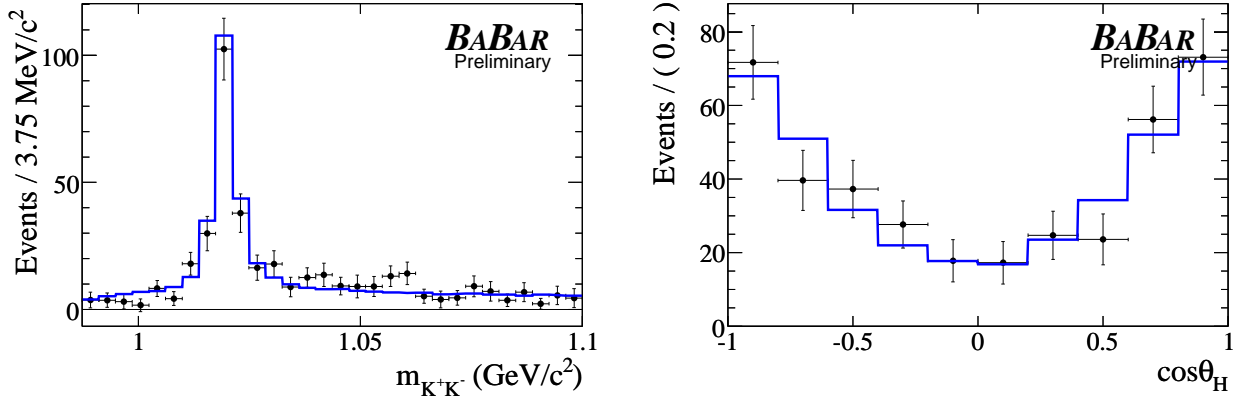


Figure 8: For the Low-mass region fit, the distributions of the Dalitz plot variables $m_{K^+ K^-}$ (left) and $\cos\theta_H$ (right) for signal-weighted data events (points) compared with the fit PDF in the $K^+ K^- K_S^0(\pi^+ \pi^-)$ mode.

uncertainty, the cleanest channel to interpret possible deviations of the CP -violation parameters from the SM expectations. Values of β_{eff} are consistent with the value found in $[c\bar{c}]K^0$ decays [5, 6].

We also calculate the parameters C and $-\eta S$ for $\phi(1020)K_S^0$ and $f_0(980)K_S^0$ using the expressions in (12) and (13). The results are shown in Table 4, along with C and $-\eta S$ for the whole DP and High-mass fits.

6 SYSTEMATIC STUDIES

We study systematic effects on the CP -asymmetry parameters due to fixed parameters in the m_{ES} and ΔE PDFs. We assign systematic errors by comparing the fit with nominal parameters and with parameters varied by their error ($\pm 1\sigma$), and assign the average difference as the systematic error. In addition, we account for a potential fit bias using values observed in studies with MC samples generated with the nominal Dalitz plot model. We take the average values of the bias observed in these studies as the systematic error. We account for fixed Δt resolution parameters, B^0 lifetime, B^0 - \bar{B}^0 mixing and flavor tagging parameters. We also assign an error due to interference between the CKM-suppressed $\bar{b} \rightarrow \bar{u}d$ and the favored $b \rightarrow c\bar{u}d$ amplitude for some tag-side B decays [32]. Smaller errors due to beam-spot position uncertainty, detector alignment, and the boost correction are based on studies done in charmonium decays. In the cases of the Low-mass and High-mass fits, we also assign systematic errors due to the isobar coefficients that are fixed to the result from

	C	$-\eta S$
Whole DP	$-0.03 \pm 0.07 \pm 0.02$	$0.77 \pm 0.09 \pm 0.02$
High-mass	$-0.05 \pm 0.09 \pm 0.04$	$0.86 \pm 0.08 \pm 0.03$
$\phi(1020)K_S^0$	$-0.14 \pm 0.19 \pm 0.02$	$0.26 \pm 0.26 \pm 0.03$
$f_0(980)K_S^0$	$-0.01 \pm 0.26 \pm 0.07$	$0.29 \pm 0.25 \pm 0.06$

Table 4: The CP asymmetry parameters C and $-\eta S$, derived using Equations (12) and (13). Results are shown for the whole DP, the High-mass region, and for both $\phi(1020)K_S^0$ and $f_0(980)K_S^0$ in the Low-mass region. For the Low-mass results, only Solution (1) is shown. The first error is statistical and the second is systematic.

the whole DP fit. In all fits we assume no direct CP violation in decays dominated by the $b \rightarrow c$ transition ($\chi_{c0}K_S^0$, $D_{(s)}K$).

We also assign an error due to uncertainty in the resonant and non-resonant line-shape parameters. The systematic uncertainty associated with the resonant component includes the uncertainty in the mass and width of the X(1550), estimated by replacing the parameters used in the nominal fit with the values found by different measurements: $m_r = 1.491$ GeV/ c^2 , $\Gamma = 0.145$ GeV [22]. All the systematic uncertainties are summarized in Table. 5.

Parameter	Whole DP		ϕK_S^0		$f_0 K_S^0$		High-mass	
	A_{CP}	β_{eff}	A_{CP}	β_{eff}	A_{CP}	β_{eff}	A_{CP}	β_{eff}
Fixed PDF Parameters	0.010	0.010	0.014	0.010	0.025	0.015	0.013	0.010
Fit Bias	0.007	0.011	0.009	0.012	0.011	0.011	0.014	0.009
DCSD, Beam Spot, other	0.015	0.004	0.015	0.004	0.015	0.004	0.015	0.004
Dalitz Model	0.005	0.005	0.009	0.002	0.060	0.024	0.027	0.023
Total	0.020	0.016	0.024	0.016	0.068	0.031	0.036	0.026

Table 5: Summary of systematic errors on CP -asymmetry parameters. Errors for ϕK_S^0 and $f_0 K_S^0$ CP -parameters are based on the Low-mass region fit. Total is obtained from the quadratic sum of the individual systematics.

7 CONCLUSIONS

We performed a ML fit to analyze the DP distribution of $B^0 \rightarrow K^+ K^- K_S^0$ decay with the full *BABAR* dataset. From a fit to the whole DP, we measure $\beta_{eff} = 0.44 \pm 0.07 \pm 0.02$, $A_{CP} = 0.03 \pm 0.07 \pm 0.02$, consistent with our previous measurements [15] and compatible with the Standard Model values $\beta \simeq 0.37$, $A_{CP} = 0$. We measure CP violation with a significance of 6.7 standard deviations (including statistical and systematic errors), and we reject the solution near $\pi/2 - \beta$ at 4.8 standard deviations.

From a fit to the region of the DP with $m_{K^+ K^-} > 1.1$ GeV/ c^2 , we measure $\beta_{eff} = 0.52 \pm 0.08 \pm 0.03$ and $A_{CP} = 0.05 \pm 0.09 \pm 0.04$, compatible with the Standard Model expectations. We measure CP violation in this High-mass region at 6.7 standard deviations.

From a fit to events at low $K^+ K^-$ masses, we measure $\beta_{eff} = 0.13 \pm 0.13 \pm 0.02$ and $A_{CP} = 0.14 \pm 0.19 \pm 0.02$ for $B^0 \rightarrow \phi(1020)K_S^0$, and $\beta_{eff} = 0.15 \pm 0.13 \pm 0.03$ and $A_{CP} = 0.01 \pm 0.26 \pm 0.07$

for $B^0 \rightarrow f_0 K_S^0$. The results for β_{eff} are roughly 1.7 standard deviations below the Standard Model value.

These results supersede our previous measurements [15] made on a smaller dataset. All of our results are consistent with our previous measurements.

8 ACKNOWLEDGMENTS

We are grateful for the extraordinary contributions of our PEP-II colleagues in achieving the excellent luminosity and machine conditions that have made this work possible. The success of this project also relies critically on the expertise and dedication of the computing organizations that support *BABAR*. The collaborating institutions wish to thank SLAC for its support and the kind hospitality extended to them. This work is supported by the US Department of Energy and National Science Foundation, the Natural Sciences and Engineering Research Council (Canada), the Commissariat à l’Energie Atomique and Institut National de Physique Nucléaire et de Physique des Particules (France), the Bundesministerium für Bildung und Forschung and Deutsche Forschungsgemeinschaft (Germany), the Istituto Nazionale di Fisica Nucleare (Italy), the Foundation for Fundamental Research on Matter (The Netherlands), the Research Council of Norway, the Ministry of Education and Science of the Russian Federation, Ministerio de Educación y Ciencia (Spain), and the Science and Technology Facilities Council (United Kingdom). Individuals have received support from the Marie-Curie IEF program (European Union) and the A. P. Sloan Foundation.

References

- [1] W.-M. Yao *et al.* [Particle Data Group], *J. Phys. G* **33**, 1 (2006)
- [2] M. Beneke, *Phys. Lett. B* **620**, 143 (2005) [arXiv:hep-ph/0505075].
- [3] G. Buchalla, G. Hiller, Y. Nir and G. Raz, *JHEP* **0509**, 074 (2005) [arXiv:hep-ph/0503151].
- [4] H. Y. Cheng, C. K. Chua and A. Soni, *Phys. Rev. D* **72**, 094003 (2005) [arXiv:hep-ph/0506268].
- [5] B. Aubert *et al.* [BABAR Collaboration], *Phys. Rev. Lett.* **94**, 161803 (2005) [arXiv:hep-ex/0408127].
- [6] K. Abe *et al.* [Belle Collaboration], [arXiv:hep-ex/0507037].
- [7] R. Itoh *et al.* [Belle Collaboration], *Phys. Rev. Lett.* **95**, 091601 (2005)
- [8] P. Krokovny *et al.* [Belle Collaboration], *Phys. Rev. Lett.* **97**, 081801 (2006)
- [9] J. Dalseno *et al.* [Belle Collaboration], *Phys. Rev. D* **76**, 072004 (2007)
- [10] B. Aubert *et al.* [BABAR Collaboration], *Phys. Rev. D* **71**, 032005 (2005) [arXiv:hep-ex/0411016].
- [11] B. Aubert *et al.* [BABAR Collaboration], *Phys. Rev. D* **74**, 091101 (2006) [arXiv:hep-ex/0608016].
- [12] B. Aubert *et al.* [BABAR Collaboration], *Phys. Rev. Lett.* **99**, 231802 (2007) [arXiv:0708.1544[hep-ex]].

- [13] J. Charles *et al.* (CKMfitter Group), *Eur. Phys. J. C* **41**, 1-131 (2005) [arXiv:hep-ph/0406184], Updated results and plots available at: <http://ckmfitter.in2p3.fr>
- [14] M. Bona *et al.* (UTfit Collaboration), *Phys. Rev. Lett.* **97** 151803 (2006), [arXiv:hep-ph/0605213], Updated results and plots available at: <http://www.utfit.org>
- [15] B. Aubert *et al.* [BABAR Collaboration], *Phys. Rev. Lett.* **99** 161802 (2007) [arXiv:0706.3885[hep-ex]].
- [16] B. Aubert *et al.* [BABAR Collaboration], *Nucl. Instrum. Meth. A* **479**, 1 (2002) [arXiv:hep-ex/0105044].
- [17] GEANT4 Collaboration, S. Agostinelli *et al.*, *Nucl. Instrum. Meth. A* **506**, 250 (2003)
- [18] M. Pivk and F. R. Le Diberder, *Nucl. Instrum. Meth. A* **555**, 356 (2005) [arXiv:physics/0402083].
- [19] H. Albrecht *et al.* [ARGUS Collaboration], *Z. Phys. C* **48**, 543 (1990).
- [20] J. M. Blatt, V. F. Weisskopf, “Theoretical Nuclear Physics”, John Wiley & Sons, New York (1952).
- [21] C. Zemach, *Phys. Rev.* **133**, B1201 (1964).
- [22] A. Garmash *et al.* [BELLE Collaboration], *Phys. Rev. D* **71**, 092003 (2005) [arXiv:hep-ex/0412066].
- [23] B. Aubert *et al.* [BABAR Collaboration], *Phys. Rev. D* **71**, 091102 (2005) [arXiv:hep-ex/0502019].
- [24] B. Aubert *et al.* [BABAR Collaboration], [arXiv:hep-ex/0605003].
- [25] B. Aubert *et al.* [BABAR Collaboration], [arXiv:hep-ex/0507094].
- [26] P. Minkowski and W. Ochs, *Eur. Phys. J. C* **39**, 71 (2005) [arXiv:hep-ph/0404194].
- [27] M. Ablikim *et al.* [BES Collaboration], *Phys. Lett. B* **607**, 243 (2005) [arXiv:hep-ex/0411001].
- [28] H. Y. Cheng and K. C. Yang, *Phys. Rev. D* **66**, 054015 (2002) [arXiv:hep-ph/0205133].
- [29] S. Fajfer, T. N. Pham and A. Prapotnik, *Phys. Rev. D* **70**, 034033 (2004) [arXiv:hep-ph/0405065].
- [30] M. Gronau and J. L. Rosner, *Phys. Rev. D* **72**, 094031 (2005) [arXiv:hep-ph/0509155].
- [31] B. Aubert *et al.* [BABAR Collaboration], *Phys. Rev. D* **72**, 072003 (2005) [arXiv:hep-ex/0507004].
- [32] O. Long, M. Baak, R. Cahn, and D. Kirkby, *Phys. Rev. D* **68**, 034010 (2003).